Dual-channel low-coherence interferometry and its application to quantitative phase imaging of fingerprints

Haniel Gabai* and Natan T. Shaked

Department of Biomedical Engineering, Faculty of Engineering, Tel Aviv University, Tel Aviv 69978, Israel
**hanielga@tau.ac.il*

Abstract: We introduce an off-axis, wide-field, low-coherence and dual-channel interferometric imaging system, which is based on a simple-to-align, common-path interferometer. The system requires no optical-path-difference matching between the interferometric arms in order to obtain interference with low-coherence light source, and is capable of achieving two channels of off-axis interference with high spatial frequency. The two 180°-phase-shifted interferograms are acquired simultaneously using a single digital camera, and processed into a single, noise-reduced and DC-suppressed interferogram. We demonstrate using the proposed system for phase imaging of fingerprint templates. Due to the fact that conventional phase unwrapping algorithms cannot handle the complex and deep surface topography imposed by fingerprint templates, we experimentally implemented two-wavelength phase unwrapping using a supercontinuum laser coupled to acousto-optical tunable filter, together functioning as a low-coherence tunable light source. From the unwrapped phase map, we produced high quality depth profiles of fingerprint templates.

OCIS codes: (090.2880) Holographic interferometry; (100.4998) Pattern recognition, optical security and encryption; (100.5088) Phase unwrapping; (120.3180) Interferometry.

References and links

1. J. Mertz, *Introduction to Optical Microscopy* (Roberts and Company Publishers, 2010), Chap.11.
2. F. Montfort, F. Charrière, T. Colomb, E. Cuche, P. Marquet, and C. Depeursinge, "Purely numerical compensation for microscope objective phase curvature in digital holographic microscopy: influence of digital phase mask position," J. Opt. Soc. Am. A **23**(11), 2944–2953 (2006).
3. N. T. Shaked, L. L. Satterwhite, M. T. Rinehart, and A. Wax, "Quantitative analysis of biological cells using digital holographic microscopy," in Holography, Research and Technologies, J. Rosen Ed., (InTech, 2011), 219–236.
4. G. C. Brown and R. Pryputniewicz, "Holographic microscope for measuring displacements of vibrating microbeams using time-averaged, electro-optic holography," Opt. Eng. **37**(5), 1398–1405 (1998).
5. E. Bonnotte, P. Delobelle, L. Bornier, B. Trolard, and G. Tribillon, "Two interferometric methods for mechanical characterization of thin films by bulging tests. Application to single crystal of silicon," J. Mater. Res. **12**(09), 2234–2248 (1997).
6. L. Xu, X. Peng, J. Miao, and A. K. Asundi, "Studies of digital microscopic holography with applications to microstructure testing," Appl. Opt. **40**(28), 5046–5051 (2001).
7. P. Chavel, "Optical noise and temporal coherence," J. Opt. Soc. Am. **70**(8), 935–943 (1980).
8. L. Martínez-León, G. Pedrini, and W. Osten, "Applications of short-coherence digital holography in microscopy," Appl. Opt. **44**(19), 3977–3984 (2005).
9. Z. Monemhaghdoust, F. Montfort, Y. Emery, C. Depeursinge, and C. Moser, "Dual wavelength full field imaging in low coherence digital holographic microscopy," Opt. Express **19**(24), 24005–24022 (2011).
10. A. A. Maznev, T. F. Crimmins, and K. A. Nelson, "How to make femtosecond pulses overlap," Opt. Lett. **23**(17), 1378–1380 (1998).
11. J. A. Ferrari and E. M. Frins, "Single element interferometer," Opt. Commun. **279**(2), 235–239 (2007).
12. A. B. Vakhtin, D. J. Kane, W. R. Wood, and K. A. Peterson, "Common-path interferometer for frequency-domain optical coherence tomography," Appl. Opt. **42**(34), 6953–6958 (2003).

#174685 - $15.00 USD Received 20 Aug 2012; revised 6 Oct 2012; accepted 7 Oct 2012; published 14 Nov 2012

13. J. A. Ferrari, E. M. Frins, D. Perciante, and A. Dubra, "Robust one-beam interferometer with phase-delay control," Opt. Lett. **24**(18), 1272–1274 (1999).
14. Q. Weijuan, Y. Yingjie, C. O. Choo, and A. Asundi, "Digital holographic microscopy with physical phase compensation," Opt. Lett. **34**(8), 1276–1278 (2009).
15. Z. Weizman, O. Vardi, and M. Binsztok, "Dermatoglyphic (fingerprint) patterns in celiac disease," J. Pediatr. Gastroenterol. Nutr. **10**(4), 451–453 (1990).
16. T. J. David, A. B. Ajdukiewicz, and A. E. Read, "Fingerprint changes in coeliac disease," BMJ **4**(5735), 594–596 (1970).
17. H. J. Weinreb, "Fingerprint patterns in Alzheimer's disease," Arch. Neurol. **42**(1), 50–54 (1985).
18. B. Seltzer and I. Sherwin, "Fingerprint pattern differences in early- and late-onset primary degenerative dementia," Arch. Neurol. **43**(7), 665–668 (1986).
19. D. Matloni, D. Maio, A. K. Jain, and S. Parabhakar, *Handbook of Fingerprint Recognition* (Springer-Verlag, 2009), Chap. 1.
20. H. Faulds, "On the skin-furrows of the hand," Nature **22**(574), 605 (1880).
21. M. C. Potcoava and M. K. Kim, "Fingerprint biometry applications of digital holography and low-coherence interferography," Appl. Opt. **48**(34), H9–H15 (2009).
22. J. Gass, A. Dakoff, and M. K. Kim, "Phase imaging without 2pi ambiguity by multiwavelength digital holography," Opt. Lett. **28**(13), 1141–1143 (2003).
23. T. Baumbach, E. Kolenovic, V. Kebbel, and W. Jüptner, "Improvement of accuracy in digital holography by use of multiple holograms," Appl. Opt. **45**(24), 6077–6085 (2006).
24. X. Kang, "An effective method for reducing speckle noise in digital holography," Chin. Opt. Lett. **6**(2), 100–103 (2008).
25. J. M. Huntley and H. Saldner, "Temporal phase-unwrapping algorithm for automated interferogram analysis," Appl. Opt. **32**(17), 3047–3052 (1993).
26. N. Warnasooriya and M. K. Kim, "LED-based multi-wavelength phase imaging interference microscopy," Opt. Express **15**(15), 9239–9247 (2007).
27. R. C. Jones, "A new calculus for the treatment of optical systems. I. Description and discussion of the calculus," J. Opt. Soc. Am. **31**(7), 488–500 (1941).
28. P. Gaom, B. Yau, J. Min, R. Guom, J. Zheng, and T. Ye, "Parallel two-step phase shifting microscopic interferometry based on ac cube beamsplitter," Opt. Commun. **284**, 4134–4140 (2011).
29. N. T. Shaked, M. T. Rinehart, and A. Wax, "Dual-interference-channel quantitative-phase microscopy of live cell dynamics," Opt. Lett. **34**(6), 767–769 (2009).

1. Introduction

In digital holography, the quantitative phase and the amplitude maps of the sample field can be numerically reconstructed from the interference pattern recorded by a digital camera [1]. Then, it is possible to use numerical calculations to compensate for aberrations, refocus, or propagate to different axial planes [1,2]. These capabilities make digital holography attractive for both macroscopic and microscopic applications, such as quantitative phase imaging of live cells and quality assurance of microstructures [3–6].

Holographic optical setups are based on interferometers, which are phase sensitive devices. This phase sensitivity can be exploited to measure high-resolution phase maps of the sample, but at the same time makes the system vulnerable to phase noise. When parasitic interferences and other noise factors are introduced to the recorded interferogram, the spectrum of the cross-correlation terms (i.e. the terms to be reconstructed) is corrupted [7,8]. In addition, the noise factors create blurring around the borders of the cross-correlation terms, making it difficult to design and fit a spatial filter for the numerical reconstruction process, due to the fact that the center and the borders of the cross-correlation terms are not clear.

These artifacts can be significantly reduced by proper design of the optical setup. For example, by using low temporal-coherence light source, most of the parasitic interferences, which are caused by multiple reflections within the optical setup and may corrupt the reconstructed data, can be significantly reduced [7,8]. However, when using such a light source in a traditional two-beam interferometer, in which the sample and reference beams creating the interference are separated in space, a rigorous and time-consuming optical-path matching between the two interferometric arms is needed to obtain interference. Moreover, if off-axis interference is used, the optical-path difference between the beams, in some regions on the camera, is longer than the coherence length of the source, resulting in degradation in the interference area, and therefore in the field of view. To achieve full-screen interference, it

#174685 - $15.00 USD Received 20 Aug 2012; revised 6 Oct 2012; accepted 7 Oct 2012; published 14 Nov 2012

is possible to tilt the field of one of the beams using a grating [9,10]. However, such a configuration requires even more rigorous alignment and is more expensive to implement.

Mechanical vibrations may add additional noise terms, and significantly defect the reliability of the resultant phase map. Due to their space-separated two arms architecture, traditional two-beam interferometers are highly sensitive to such vibrations, and therefore, sterile and stable environment is required (i.e. floating optical tables and acoustical housing boxes). Such conditions further increase the cost of the imaging system and restrict its portability [11–13]. Another problem with the traditional two-beam interferometers is different beam curvatures in the two interferometric arms. The Linnik's interferometric configuration solves this problem by introducing the same curvature to the sample and reference waves, but decreases the system stability due to the need for an additional microscope objective [11,14]. Another possibility is to use numerical compensation methods, but these may add significant computational complexity to the reconstruction process [2].

An alternative design, which is less sensitive to mechanical vibrations, is the common-path interferometer [11–14]. Ferrari *et al.* [11] suggested such an interferometer, which is based on a single cube beamsplitter. This design reduces the number of optical elements needed, as well as lowers the sensitivity for mechanical vibrations. Weijuan *et al.* [14] showed that this design also has inherent wavefront-curvature compensation.

In the current paper, we suggest a low-coherence, common-path interferometric imaging system, which is based on a single cube beam splitter and a supercontinuum fiber laser source coupled to acousto-optical tunable filter, having the attractive advantages of wide-field, low-coherence, common-path and dual-channel interferometric imaging all together. The new hybrid system is easy-to-align and requires no beam-path matching for obtaining interference with a low-coherence source, in contrast to other types of interferometers. In addition, the proposed system produces immediate off-axis interference with high spatial frequency on each of the two channels, recorded simultaneously by a digital camera, with minimal degradation in the field of view. The two simultaneous and naturally 180°-phase-shifted interference channels can be used for various applications. In the current paper, we used these two channels to obtain a single, noise-reduced and DC-suppressed interferogram.

The proposed system will be demonstrated in resolving highly accurate depth profiles of fingerprint templates (FPTs). Such application holds great potential for both biomedical and biometrical purposes [15–20]. However, phase imaging of FPTs with digital holographic systems is a challenging task. The FPT surface topography varies from tens to hundreds of microns [21], resulting in complex wrapped phase maps that most of the digitally implemented unwrapping algorithms fail to handle. To overcome this problem, we used a two-wavelength phase unwrapping method, which is capable of handling such complex and deep topographies [22]. To acquire the sample in two wavelengths, we took advantage of the tunable low-coherence laser in choosing the two central wavelengths.

2. System configuration

The proposed system is illustrated in Fig. 1(a). A temporally low-coherence supercontinuum fiber laser source (SC-400, Fianium, coupled to acusto-optical tunable filter, with FWHM spectral bandwidth of ~6nm) is spatially filtered by a 25 μm pinhole, while expended by two 4f systems containing four achromatic lenses ($L_{0\text{-}3}$) with focal lengths of 35, 50 25, and 150 mm, respectively, creating an expended collimated beam with a diameter of 1". Half of the illuminating beam interacts with the sample (FPT in our demonstration) and serves as the interferometric sample arm. The second half of the beam, which passes through the empty slide, serves as the interferometric reference arm. A third achromatic 4f lens system ($L_{4,5}$) delivers the amplitude and the phase of the sample to the lower half of the beamsplitter (BS), and non-diffracted plane waves from the empty, upper part of the sample plane to the upper half of the BS. The BS diagonal plane is slightly tilted from the optical axial. This way, the BS serves as a common-path interferometer and creates two 180°-phase-shifted

#174685 - $15.00 USD Received 20 Aug 2012; revised 6 Oct 2012; accepted 7 Oct 2012; published 14 Nov 2012

interferograms on the camera plane in parallel. The camera used is the DCC1545M CMOS camera from Thorlabs with 1280 × 1024 square pixels of 5.2μm each. For each interferogram, a wedge-shaped optical path delay is created between the transmitted and reflected light beams within the BS, enabling the off-axis interference pattern as shown in Fig. 1(b). The off-axis spatial frequency of the interference pattern is determined by the angle θ between the optical axis and the diagonal semi-transparent surface of the BS. As illustrated in Fig. 1(b), when increasing the angle θ, the interference frequency increases accordingly. Both the camera and the light source are controlled and synchronized via LabView in order to enable fast acquisition of the FPT in multiple wavelengths, which is helpful in implementing the two-wavelength phase-unwrapping method explained next.

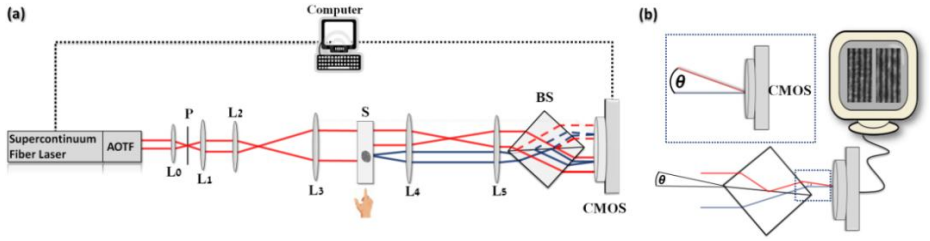

Fig. 1. (a) Low-coherence, dual-channel common-path interferometric imaging system, used for fingerprint templates imaging. L0-5 - achromatic lenses, P - 25 μm, pinhole, S - sample, BS - beamsplitter. Blue lines - sample arm, red lines - references arm. Solid lines - left channel, dashed lines - right channel. CMOS - CMOS digital camera which is synchronized with the light source by a computer. (b) Schematic of the interference creation upon one channel, where θ is the angle between the optical axis and the semi-transparent surface of the BS.

This simple common-path, low-coherence interferometer holds great advantages for holographic and interferometric imaging. First, due to its common-path geometry, the interferometer is more stable and less sensitive to vibrations than traditional interferometers (i.e. Mach-Zehnder, Michelson, etc), as well as automatically compensates for wavefront curvature distortions. Second, since we use a low-temporal-coherence light source, coherent noise is significantly reduced. One of the greatest advantages of the proposed system is its simplicity in obtaining interference using a low-coherence source without difficult alignment and without degradation in the field of view, where the length of the interference area is only limited by the coherence length of the source and by the interference angle. The interference angle θ determines the interference length L on the camera as follows [9]: $L = \lambda_0^2/[2\sin(\theta/2)\cdot\Delta\lambda]$, where λ_0 is the central wavelength and $\Delta\lambda$ is the spectral bandwidth. In our case, we used λ_0 = 633 nm, $\Delta\lambda$~6nm and θ~1.66°, so we got L~443 pixels, and obtained straight off-axis interference with 4.2 pixels per interference cycle on the area of each channel (1000 × 443 pixels of 5.2 μm each) immediately, without beam-path matching.

3. Quantitative fingerprint imaging

There are scientific evidences that fingerprint patterns may serve as a simple, non-invasive bio-marker for Coeliac and Alzheimer disease. Coeliac patients have shown significant feature changes in their fingerprints morphology. These changes are characterized by moderate epidermal ridge atrophy and, in some cases, even complete loss of the fingerprint pattern. In addition, it has been shown that newly diagnosed patients, who suffered from severe ridge atrophy, had almost complete reconstruction of their fingerprint pattern after the appropriate treatment [15,16]. There are also evidences that fingerprint patterns may serve as an early indicator for Alzheimer disease, where patients had shown significantly differently features related to their fingerprint morphology in comparison to healthy control groups [17,18]. Exploring three-dimensional FPTs of such patients may provide additional pathologic information in a simple noninvasive manner. For biometrical applications, fingerprint recognition is one of the oldest and most widely used authentication methods

#174685 - $15.00 USD Received 20 Aug 2012; revised 6 Oct 2012; accepted 7 Oct 2012; published 14 Nov 2012

[19,20]. Quantitative phase imaging offers several unique advantages for fingerprint biometrics. By providing imaging of both two and three-dimensional structures with sub-micrometer resolution, identity theft and spoofing become more complex to achieve. In addition, blurring distortions, inherent in the creation process of the FPTs, can be repaired by thresholding on depth values, which is not possible for the traditional FPT imaging techniques using ink.

3.1 Sample preparation

To achieve high quality FPTs, we have examined several transparent materials, such as water, oil, liquid glue, soap, and ultrasound gel. We have finally chosen to use an ultrasound gel since it had the most impressive performances in keeping the template shape without deformation, in addition to its transparency and nontoxicity. To create the template, a thin layer of ultrasound gel (AquaSonic Clear, n_{gel} = 1.3535) is spread on the experimenter finger using a cotton swab, and pressed against half of a microscope cover-glass (~0.15 mm thick). The sample is placed on a mount and the two interferograms are recorded together.

3.2 Dual-interferogram reconstruction

The proposed configuration simultaneously provides two interferograms, which are naturally phase shifted by 180° (see Fig. 2(a)). We utilize these interferograms to obtain a single, noise-reduced and DC-suppressed interferogram. After a slight registration and a digital intensity calibration between the two interferograms (since the BS does not necessarily transmit and reflect the same amount of intensity), we defined the new interferogram by subtracting one of the interferograms from the other one, and dividing the product by 2. As it can be seen from the spatial spectra in Fig. 2(c), the new interferogram has a significantly reduced DC term, which is a result of the subtraction between the DC terms of each channel divided by two. Second, the cross-correlation terms were averaged and blurring around these terms is significantly reduced (see Fig. 2(c)) [23,24]. This is important in our case since the two-wavelength phase unwrapping method, presented next, is highly sensitive to noise.

3.3 Two-wavelength optical phase unwrapping

By the appropriate spectral analysis of the new interferogram (off-axis digital reconstruction process, which is fully detailed in [1]), it is possible to calculate the quantitative phase map of the sample. However, the phase profile is wrapped and contains 2π ambiguities in places where the optical thickness of the sample is greater than the central wavelength of the illuminating source [22]. In some cases, digital unwrapping algorithms can detect and repair such ambiguities [25]. However, these algorithms cannot handle complex surface with deep topographies, such as the one of the FPT. To overcome this problem, we used a two-wavelength unwrapping method suggested by Gass *et al*. [22]. This method is based on the acquisition of two interferograms in two different wavelengths λ_1 and λ_2, followed by subtraction of the two phase maps of each wavelength. Next, a few simple mathematical manipulations with λ_1 or λ_2 are performed, as fully described in [22]. The final result yields a new phase map, where its effective beat wavelength is $\Lambda_{12} = \lambda_1\lambda_2/|\lambda_1 - \lambda_2|$, so that the beat wavelength can be increased by choosing close wavelengths. It should be noticed that the amplification of each of the wavelengths, λ_m; m = 1,2, results in an amplification of the phase noise term $2\pi\varepsilon_m$ in the phase map ϕ_m by a factor equals to the amplification of λ_m. For this unwrapping method to work properly, the maximum noise level must obey the following condition [22,26]: $\varepsilon_m < \lambda_m /4\Lambda_{12}$; ($m$ = 1,2). Using the proposed system and a wise selection of wavelengths, we produced a high quality depth profiles using two wavelengths only. The wavelengths used were λ_1 = 633nm and λ_2 = 636nm, which creates a beat wavelength of Λ_{12} = 134196nm. Therefore, in our case, noise terms ε_1 and ε_2 have to stay below level of 1%.

#174685 - $15.00 USD Received 20 Aug 2012; revised 6 Oct 2012; accepted 7 Oct 2012; published 14 Nov 2012

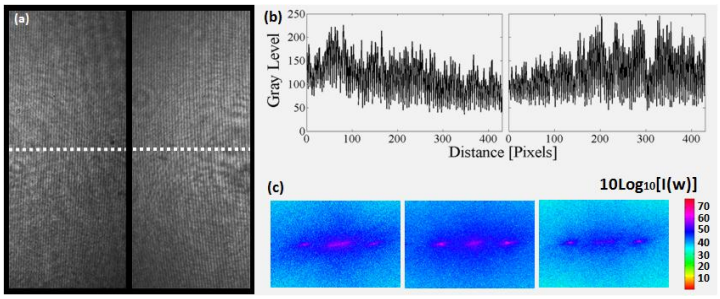

Fig. 2. (a) Dual-channel, off-axis interference pattern with 4.2 pixels per cycle (1000 × 443 pixels per channel). (b) Cross-section of the interference channels in the location marked by a white dashed line in (a). (c) Intensity spectrum in logarithmic scale of the left interferogram (left), the right interferogram (middle), and the new interferogram (right). The DC term is significantly suppressed and the blurring around the cross-correlation terms is reduced.

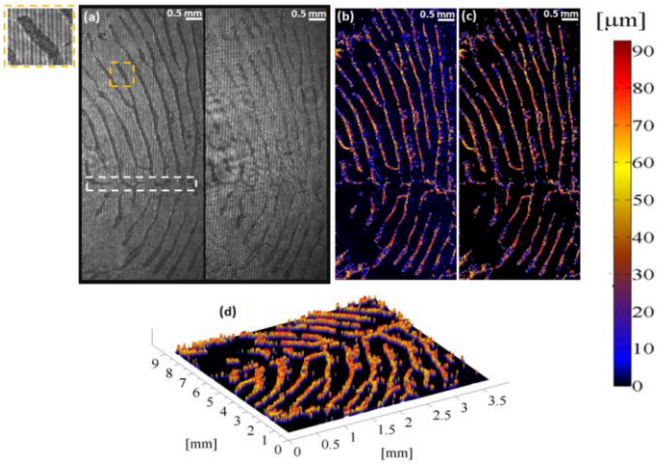

Fig. 3. (a) Two 180°-phase-shifted interferograms of the FPT, acquired simultaneously. The dashed white square indicates on the scar location. (b) Depth profile distorted by blurring (in blue). Significant distortion can be seen in the upper-right part of the image. (c) Final result with improved contrast. (d) Final result in three-dimensional view.

3.4 Experimental results

A FPT was taken from the distal part of the experimenter's right thumb, where he has a slight scar interrupting with the continuity of the arches morphology. At first, we acquired and registered the two 180°-phase-shifted interferograms shown in Fig. 3 (a), followed by the reconstruction and unwrapping stages. From the quantitative phase map, we have decoupled the depth profile of the sample (Figs. 3(b-d)), under the assumption that the refractive index of the ultrasound gel is constant (n_{gel} = 1.3535). From these depth profile, we see that there are no ambiguities and that most of the FPT thickness values vary around 65-90µm.

Blurring distortions are caused by gel residuals and clearly seen in Fig. 3(b) in blue between the ridges of the FPT. We noticed that their thickness vary from 2 to 10 µm, which is way below the values of the FPT surface topography. By applying a threshold on the depth values, possible only because we used interferometry, we significantly reduced the blurring while improving the imaging contrast (see Figs. 3(c) and (d)).

4. Conclusion and future work

We introduced a new, low-coherence, dual-channel interference imaging system, which is based on easy-to-align, common-path interferometer. It requires no optical-path matching as in a traditional two-beam interferometer, creates interference with minimal degradation in the

#174685 - $15.00 USD Received 20 Aug 2012; revised 6 Oct 2012; accepted 7 Oct 2012; published 14 Nov 2012

field of view, and physically compensates for wavefront curvature distortions. We have used a unique algorithm which takes advantage of the dual-channel property to create a single, DC-suppressed and noise reduced interferogram. In addition, due the flexibility granted by the tunable light source and using experimentally-implemented, two-wavelength phase unwrapping, we could handle complex and deep phase topographies. Though we have used this system to image fingerprint templates, it holds great potential for both microscopic and other macroscopic applications. Additionally, by simple modifications, the two channels can be used for obtaining two orthogonal polarization states (to derive the full polarization state in each pixel by Jones formalism) [27], or to acquire two wavelengths in a single camera exposure [22]. Furthermore, the dual-channel property of this low-coherence interferometer might find use for phase-shifted holography [28] and for slightly off-axis holography [29].

Acknowledgments

This work was supported by the Israel Science Foundation (ISF) Bikura Grant.

#174685 - $15.00 USD Received 20 Aug 2012; revised 6 Oct 2012; accepted 7 Oct 2012; published 14 Nov 2012